


Article

Spatiotemporal Evolution Characteristics of Apparent Resistivity and Its Response Correlation with Acoustic Emission of Coal under Multi-Step Loading

Xinyu Wang ¹, Guoqing Zhu ¹, Deqiang Cheng ², Bin Miao ^{3,*}, Fanbao Chen ¹ and He Tian ¹¹ School of Safety Engineering, China University of Mining and Technology, Xuzhou 221116, China² School of Information and Control Engineering, China University of Mining and Technology, Xuzhou 221116, China³ School of Resources and Geosciences, China University of Mining and Technology, Xuzhou 221116, China

* Correspondence: zymb@cumt.edu.cn

Abstract: To understand the early warning signs of damage during the coal mass deformation process, an integrated monitoring procedure was designed that combines the apparent resistivity (AR) and acoustic emission (AE) of coal damage under multi-step loading. The spatiotemporal response characteristics of AR and the time-varying evolution of AE were studied and the varying correlation between the two was discussed. Additionally, the macro–microscopic mechanics of the AR response during the coal deformation process was explored. The results show that the AR and AE signals corresponded well with the applied load during the coal deformation process. In the early loading stage, variations in AR and AE signals were not apparent. As the applied load increased, the high-resistance area of AR increased and the AE signals became active. The local variation characteristics of AR could be used to indirectly invert the internal structure of the coal samples. The electrical variation in the loaded coal was mainly controlled by the conductive surface of cracks. The acoustic and resistivity methods can strongly complement the spatial and temporal dimensions of early warning systems for disasters. The AE technique can continuously monitor a test area for abnormal occurrences in the engineering site, and AR tomography images that are obtained can be used to locate inversions in the source coal in order to take pre-emptive action before disaster occurs. This research can provide new ideas for monitoring and early warning systems for coal and rock dynamic disasters.

Keywords: multi-step load; acoustic emission; resistivity method; coal fracture; spatiotemporal evolution; early disaster warning



Citation: Wang, X.; Zhu, G.; Cheng, D.; Miao, B.; Chen, F.; Tian, H.

Spatiotemporal Evolution Characteristics of Apparent Resistivity and Its Response Correlation with Acoustic Emission of Coal under Multi-Step Loading. *Sustainability* **2022**, *14*, 10061. <https://doi.org/10.3390/su141610061>

Academic Editors: Xiangguo Kong, Dexing Li and Xiaoran Wang

Received: 16 July 2022

Accepted: 4 August 2022

Published: 14 August 2022

Publisher's Note: MDPI stays neutral with regard to jurisdictional claims in published maps and institutional affiliations.



Copyright: © 2022 by the authors. Licensee MDPI, Basel, Switzerland. This article is an open access article distributed under the terms and conditions of the Creative Commons Attribution (CC BY) license (<https://creativecommons.org/licenses/by/4.0/>).

1. Introduction

With the increasing intensity and depth of coal mining in China, coal–rock dynamic disasters, such as rock burst, roof fall, and coal and gas outburst, are becoming more serious [1]. A coal–rock dynamic disaster is a complex process in which internal microfractures develop and multiply under external load perturbation until visible damage is produced [2–4]. Therefore, studying the evolution characteristics of coal mass deformation and rupture in different loading stages and accurately capturing the early warning signs of damage could provide a theoretical and methodological basis for disaster prediction and prevention at engineering sites. At the same time, the process of coal mass rupture produces a variety of physical effects, such as changes in AE, electrical signals, and other physical information [5–7]. In addition, joint monitoring and multi-source information analysis by various means could help us more thoroughly understand the early warning signs of coal mass deformation and rupture and solve the limitation that single sources of information cannot accurately identify disaster sources.

AE is a phenomenon in which tiny cracks that exist inside a material close under external loading and energy is released in the form of elastic waves when new cracks develop, expand, and penetrate [8]. Recently, many scholars have conducted extensive research on AE signals during the coal mass loading process. Jia et al. revealed the spatial and temporal evolution characteristics of coal damage during this process by studying the physical behavior and AE signals of coal at different depths under triaxial compression conditions [9]. Li et al. adopted the Hilbert–Huang transform (HHT) method to examine the detailed structural characteristics of coal masses that were damaged at different loading stages by analyzing AE waveform characteristics [10]. Dou et al. conducted uniaxial compression tests on sandstone samples that involved pre-cracking at different dip angles and investigated the effect of the crack dip angle on the fracture mechanism using AE and scanning electron microscopy (SEM) [11]. Zhang et al. analyzed the AE signals of coal samples under true triaxial loading and unloading during the process of deformation and failure and found that the multifractal characteristics of AE were able to reflect the degree of stress and damage in the coal samples [12]. Feng et al. studied the fracture characteristics of coal mass under dynamic loading and the AE signal response and found that the dynamic intensity was bimodal. In addition, the AE peak counts and energy increased linearly with the impact velocity but decreased with increased axial static load [13]. Kong et al. studied the variance and autocorrelation coefficients of AE signal sequences by introducing critical moderation theory [14]. Li et al. conducted uniaxial compression experiments on sandstone samples with different water content and collected AE signals. They found that the water content significantly affected the mechanical behavior and AE signals of the sandstone samples [15]. Through AE monitoring, Wang et al. conducted quantitative inversion of the source mechanism of rock fracture and obtained the spatiotemporal evolution law of the source parameters, such as microcracking type, fracture size, azimuth orientation, dissipated energy, etc. [16]. The passive and real-time AE monitoring technique has irreplaceable advantages in coal and rock fracture monitoring.

Resistivity is one of the important physical parameters of coal mass, and there have been many in-depth studies on the variation law of the resistivity of coal under different conditions. Jiang et al. studied the variation in the resistivity of quartz sandstone and limestone under uniaxial loading conditions and introduced Maxwell's conductivity formula to analyze those variations during experiments [17]. Li et al. derived and tested an analytical expression for the damage variables of rock samples based on resistivity characterization and obtained the damage evolution equation for typical rock samples. They also proposed discrimination criteria and pre-damage characteristics for the damage state of rock samples [18]. Jia et al. studied the variation in resistivity response during the process of crack development, expansion, and merging in saturated green sandstone under uniaxial loading and proposed a method for fracture potential prediction based on resistivity anisotropy [19]. Liu et al. investigated the AR of coal samples during the process of uniaxial loading. The correspondence between AR and stress was also analyzed to reveal the mechanism of AR response to coal damage [20]. Xu et al. conducted Brazilian splitting tests on two groups of vertical and parallel limestone samples and obtained the resistivity law for two loading modes. Their test results proved the evolution law for resistivity damage variables [21]. The above results all show that the resistivity method can effectively reflect the characteristics of deformation and rupture during coal loading, which is one of the main methods used for active geophysical exploration in mines.

The above research shows that the study of resistivity change in loaded coal mass has mainly been limited to the temporal variation characteristics of resistivity, and the spatial variation characteristics during the loading process have been less studied. In addition, it is difficult to monitor electrical signals throughout the whole process of coal mass loading in real time due to the limitation of sampling frequency of the measuring instrument. Moreover, while the AE technique can monitor the test area in real time and is sensitive to the moment of coal mass rupture, compared with the active detection technique, the main disadvantage of AE for dynamic disaster prediction is that the advance time is not

long enough. In other words, when the AE signal is detected, the damage or fracture has already occurred, while an active detection technique such as resistivity can predict the risk in advance, before the disaster occurs, and it is difficult to reflect the internal evolution state of the coal mass during the loading process in all aspects. The two observation methods, AE and resistivity, both have their advantages, but the correlation between them in the spatial and temporal dimensions of coal fracture warning still needs to be further clarified.

This paper integrates the DC resistivity method and the AE technique to test the AR and AE signal response laws during the multi-step coal mass loading process. The focus is on analyzing the spatial and temporal evolution characteristics of the AR of the coal mass to reveal the change mechanism from the microscopic and macroscopic perspectives. By exploring the spatial and temporal correlation of the AR-AE response to the coal damage process, a new idea for dynamic disaster warning based on the integration of passive monitoring and active detection is proposed. The research results provide an important theoretical foundation and experimental basis for further clarifying the evolution of coal rupture damage and enriching the technical system of dynamic disaster monitoring, prevention, and control.

2. Experimental Preparation and System

2.1. Sample Preparation

The coal samples were taken from the 11061-machine tunnel of the Fangshan coal mine in Yuzhou City, Henan Province, China. The coal samples were processed by a method recommended by the International Society for Rock Mechanics and Rock Engineering (ISRM). Standard specimens with a diameter of 50 mm and height of 100 mm were used, and non-parallelism and non-perpendicularity were controlled to within ± 0.05 mm. A total of 18 coal samples were used, numbered sequentially from M-1 to M-18. To facilitate the analysis, the basic parameters of the tested coal mass were analyzed industrially, and the results are shown in Table 1. The tested coal was relatively soft, with the following properties: density $\rho = 980$ kg/m³, Poisson's ratio $\nu = 0.26$, Young's modulus $E = 1.2$ GPa, and uniaxial compressive strength (UCS) = 4.2 MPa. The p -wave and S-wave velocity were 1180 and 670 m/s, respectively.

Table 1. Basic parameters of coal samples.

Parameters	Moisture ($M_{ad}/\%$)	Ash Content ($A_d/\%$)	Volatile Fraction ($V_{daf}/\%$)
Value	1.15	7.32	12.20

2.2. Experimental System

The experimental coal mass AR–AE system mainly included four parts: loading system, shielding system, AE acquisition system, and electrical parameter acquisition system, as shown in Figure 1.

The experimental loading system consisted of a SANS-Y4306 electro-hydraulic servo press platform. The platform was mainly composed of a servo press, a DCS loading control box, and a PowerTest V 3.3 control program, with maximum load capacity of 3000 kN and data acquisition frequency up to 20 Hz. Three loading methods could be realized: force control, displacement control, and constant load control.

The experimental shielding system consisted of an AFGP-II high-efficiency shielding room, with a shielding range of 50 MHz–1 GHz ≥ 110 dB, 300 kHz ≥ 110 dB, 100 kHz ≥ 100 dB, and 14 kHz ≥ 80 dB to meet the shielding requirements of the experiment. In order to avoid the conduction of excitation current to the press during electrical detection, insulating paper was placed at the upper and lower ends of the coal mass prior to the experiment to avoid direct contact with the press and ensure the accuracy of the test results.

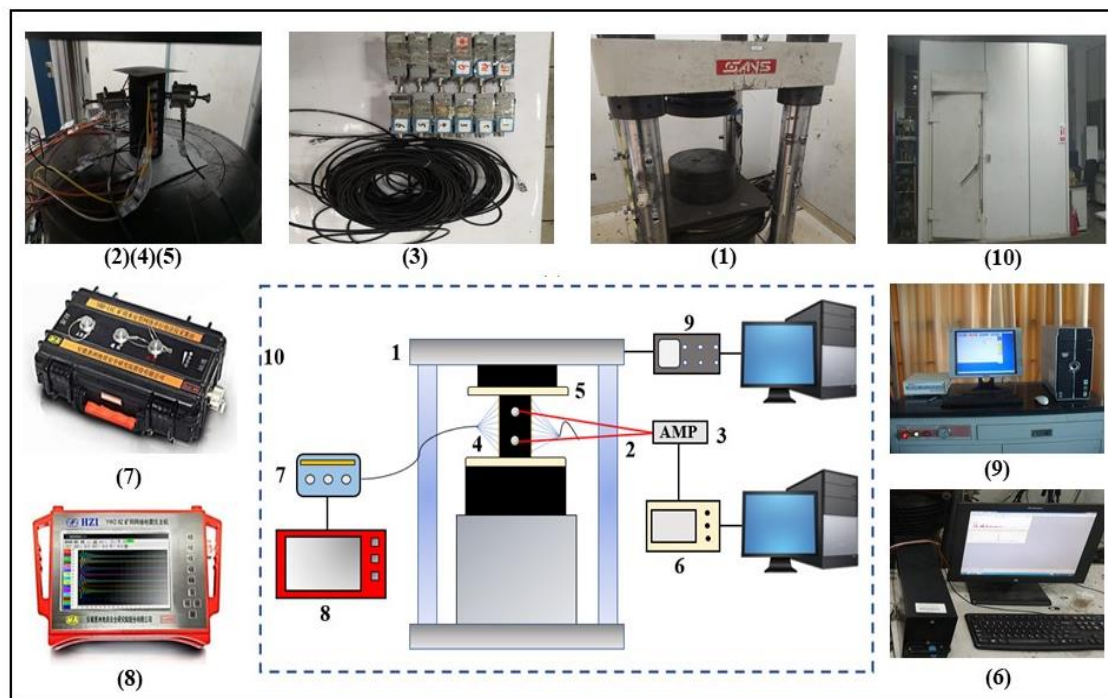


Figure 1. Experimental system: (1) press head; (2) AE probe; (3) preamplifier; (4) electrodes; (5) insulating paper; (6) AE data acquisition system; (7) acquisition base station; (8) electrical method host; (9) press control system; (10) shielding room.

The AE acquisition system was a PAC-II system from Physical Acoustics, USA. The system consists of an A/D converter module, pre- and gain amplifiers, and waveform processing module, which can realize efficient acoustic signal acquisition using multiple channels (up to 32) by computer. In order to ensure that there is no interference between channels, a preamplifier is connected to each channel through a shielded line. Two Nano-30 miniature AE sensors (diameter = 8 mm; height = 8 mm) with a resonant response at 300 kHz were used in the experiments to measure the time-varying parameters (i.e., AE counts) during the deformation process of loaded coal specimens. The AE sensors are placed in the special fixture, and the fixture chuck is glued to the surface of the sample by hot-melt adhesive.

The electrical parameter acquisition system consists of a Huizhou Institute YBD-11Z type network parallel electrical method host, acquisition base station, and patch electrodes. The signal acquisition of the instrument can reach up to 64 channels, the measuring voltage accuracy is ± 0.3 mV, and the sampling interval can be set from 1 to 20 ms. The pure copper patch electrode is 7 mm long, 4 mm wide, and 0.5 mm thick, and is fully coupled with the sample by conductive epoxy adhesive and connected to the acquisition base station by silver-plated shielding wire.

2.3. Experimental Schemes and Procedures

In this study, uniaxial multi-step loading was used, the loading control method was force-controlled, the rate was set to 20 n/s, and the step load was maintained for 30 s with increments of 1 kN. The AE acquisition parameters were assigned as sampling frequency of 20 MHz and amplification of 40 dB. The electrodes were arranged in a two-dimensional symmetric arrangement, as shown in Figure 2. The electrical parameters were collected using the AM method with a power supply time of 0.1 s and a sampling interval of 10 ms. The mechanical parameters, AE signals, and electrical parameters of the coal sample were collected simultaneously during the whole loading process.

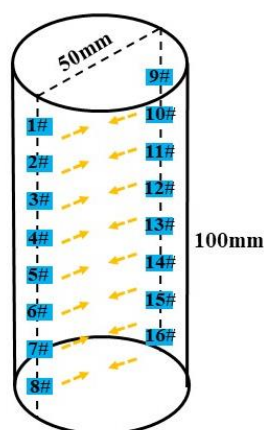


Figure 2. Electrode arrangement.

After the acquisition, the data processing was mainly done by the parallel electro fabrication instrument with WBD 3.0 analysis software. First, the data were imported into the software and preprocessed through the main interface to reject distortion points and bad data. Then, the coordinates were set according to the actual position of the electrode in the 3D space, and the space type and device type were entered. Next, the measurement line was segmented, and the appropriate azimuth and inclination angles were set to form a symmetric profile. Finally, the AR values were calculated and plotted into an AR tomography image.

3. Analysis of Experimental Results

3.1. Analysis of Variation Characteristics of AR and AE

According to the characteristics of the time–load curve, the AR of each sample during the dead load and the unloaded moment was extracted for calculation, and then drawn in an AR tomogram and marked. Tomograms with similar AR data were marked with the same color scale, and the AE counts of the whole loading process were extracted for comparative analysis. Due to space limitations, two representative samples, M-3 and M-11, were selected for description, and the analysis of sample M-3 is emphasized.

The temporal characteristics of AE counts during the multi-step loading of sample M-3 and the changing pattern of tomography images of AR evolution at different stages are shown in Figures 3 and 4. It can be seen that native microscopic cracks in the coal mass gradually closed to form new conductive channels under the action of axial stress at the early stage of loading, resulting in the development of a low-resistance point-like potential in the original strip-like central high-resistance imaging area with increasing load. However, due to the low stress level, the overall structure of the sample did not undergo extensive pose adjustment, so the chromatic aberration of the tomography imaging map changed slowly and the low-resistance region still dominated. The AE counts did not produce significant changes; only discrete signals were generated by the influence of microscopic crack closure in the late stage of this phase, which were maintained at a low level.

At the late stage of loading, the AR tomography image started to show divergent behavior; the left and lower resistance values had complete convergence and produced a significantly increased resistance value, while the central high-resistance area continued to spread and produced signs of penetration in the lower part. At this time, the microscopic fracture development inside the coal mass moved from disorderly to orderly and the expansion speed accelerated sharply, forming a macroscopic main rupture and irreversible damage by converging with and penetrating the primary fracture. When the current flowed through the rupture area, conductivity decreased and the high-resistance imaging area filled the interior of the profile compared with the previous stages. At this stage, the AE signal intensity increased significantly, the counts increased sharply and intensely, and a sudden increase occurred near the stress peak while reaching the instantaneous maximum.

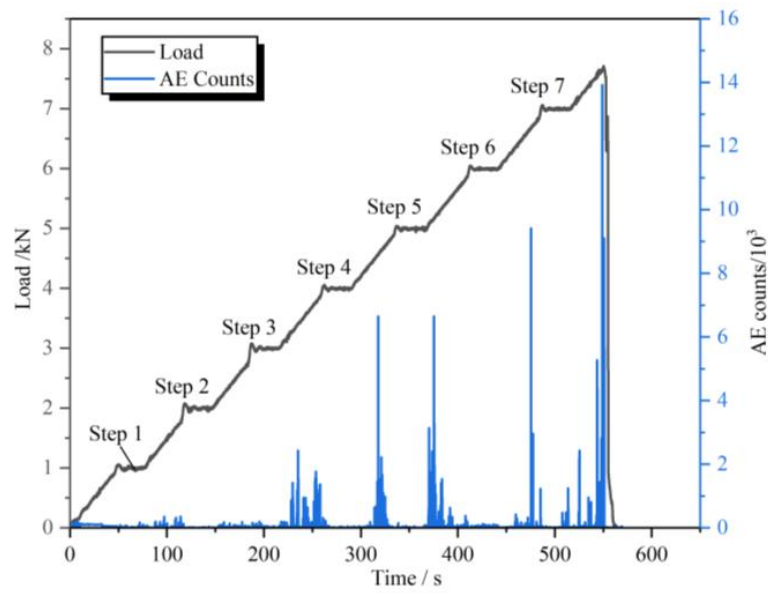


Figure 3. Relationship curves of time–load and AE rate for sample M-3.

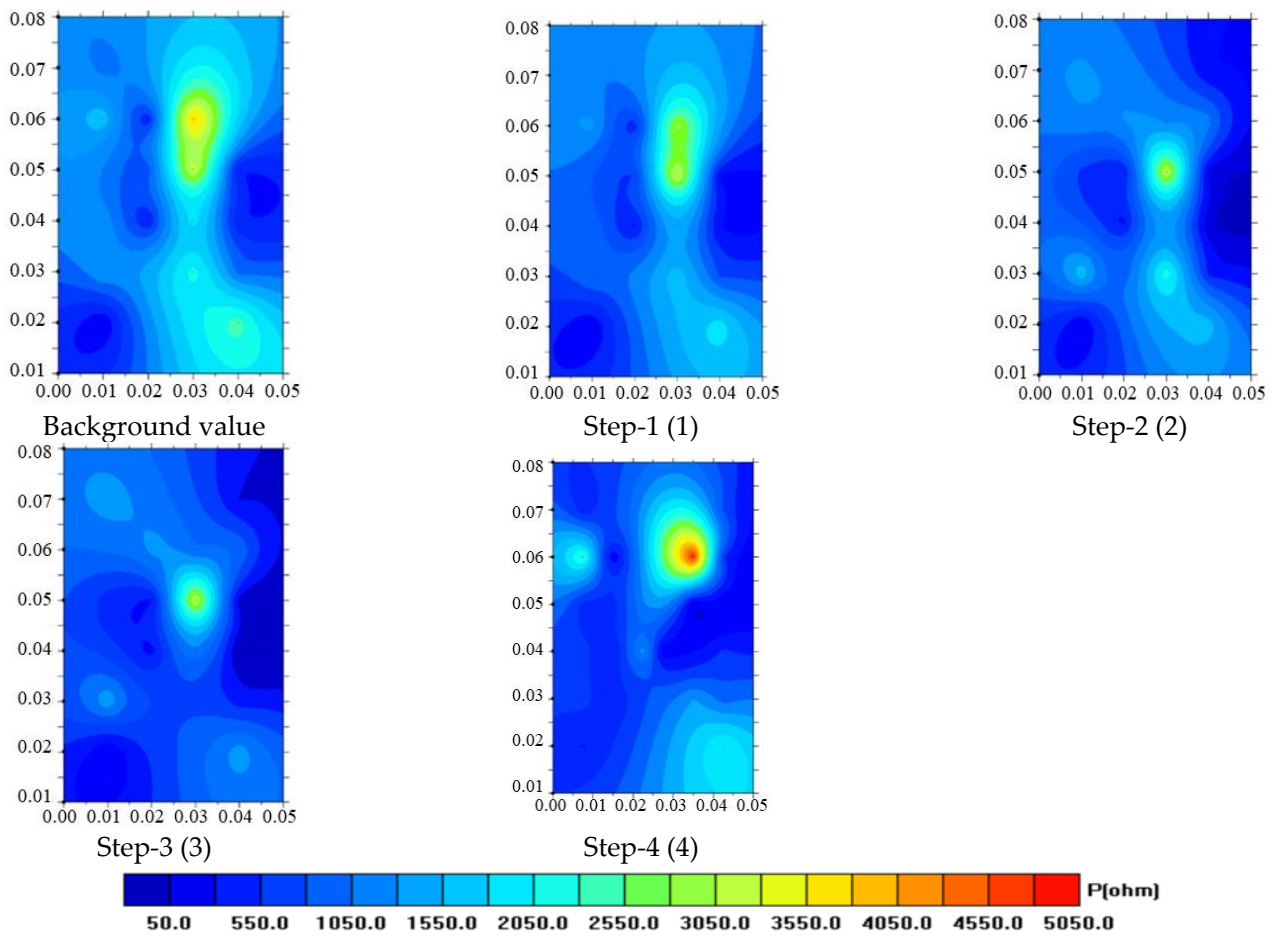


Figure 4. Cont.

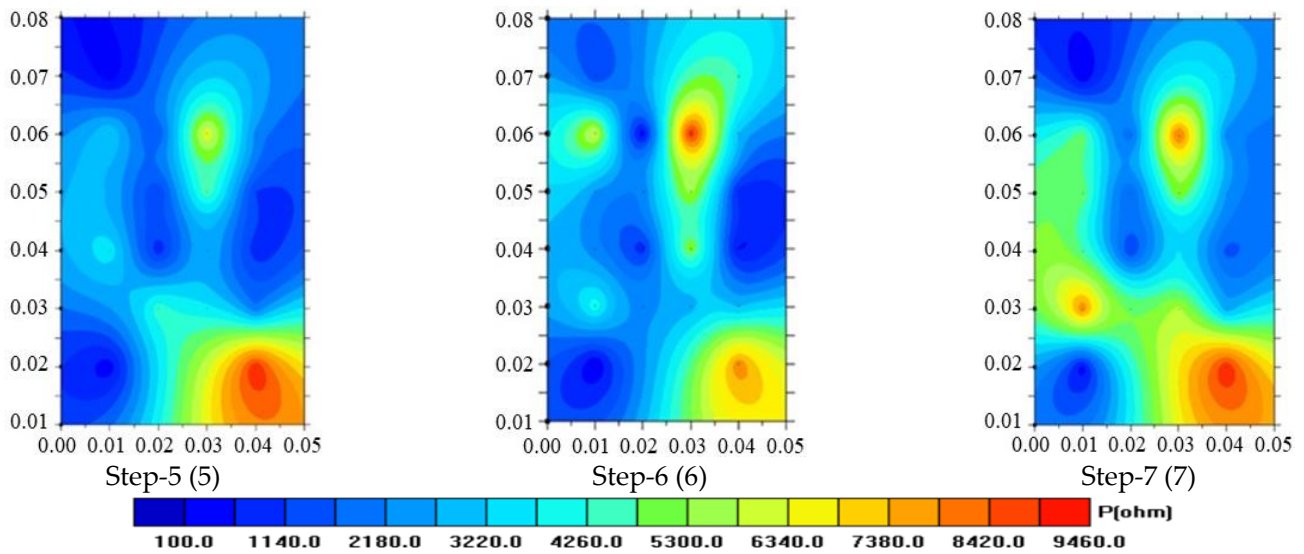


Figure 4. Tomography images of AR evolution of sample M-3 at different dead load stages.

The temporal characteristics of AE counts during the multi-step loading of sample M-11 and the changing pattern of tomography images of AR evolution at different stages are shown in Figures 5 and 6. It can be seen that the AR and AE counts of sample M-11 had similar evolution laws compared with sample M-3. For AR, in the initial loading stage, the high-resistance region showed a decreasing trend due to the effect of primary fracture closure. With the gradually increasing load, AR gradually increased under the influence of fracture development and confluence inside the coal sample. At the same time, the relatively high-resistance area continued to expand with increasing load-bearing degree in the middle and late stages of the loading process, producing a magnitude change. In addition, the AE response and stress change also maintained good consistency. When the coal load increased one level, the active degree of AE counts increased, but in the dead load stage, the AE counts were very weak and a quiet period appeared. Altogether, the overall experience can be roughly divided into three stages: stable silence area, intermittent pulse area, and rapid increase area.

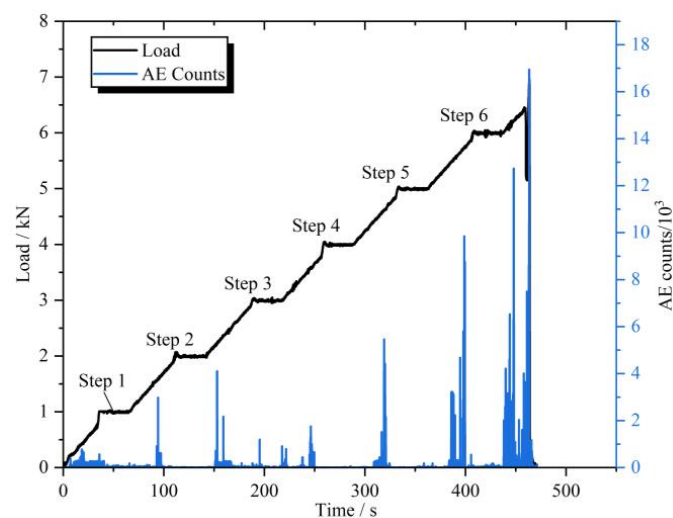


Figure 5. Relationship curves of time with stress and AE rate for sample M-11.

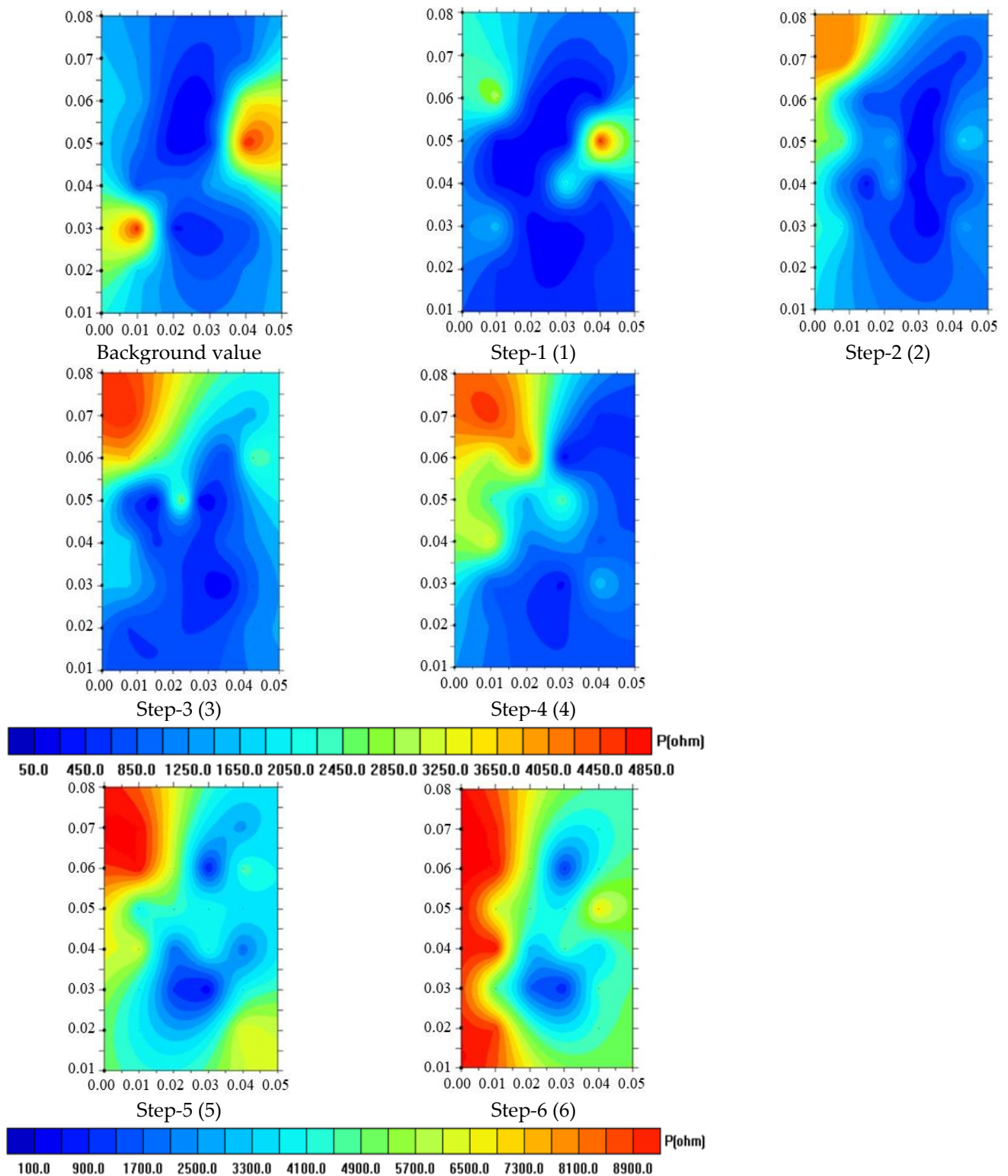


Figure 6. Tomography images of AR evolution of sample M-11 at different dead load stages.

3.2. Analysis of Time Series Variation Characteristics of AR

In order to gain further insight into the time-varying law of local AR during the deformation process of loaded coal samples, some key points with high resistance and obvious AR variation were selected within the tomography image, marked as A–F in

Figures 7 and 8. Then, the time-varying characteristics of AR response at these key points were extracted, and the results are shown in Figures 9 and 10.

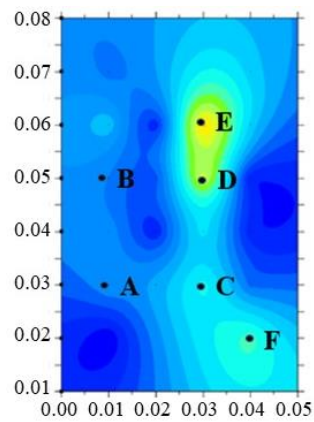


Figure 7. Position of each point of sample M-3.

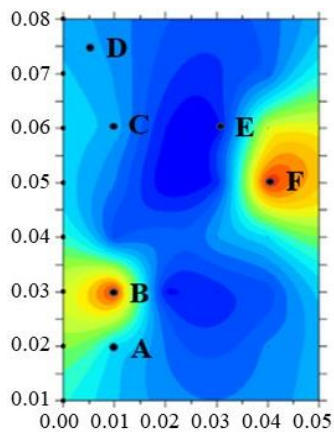


Figure 8. Position of each point of sample M-11.

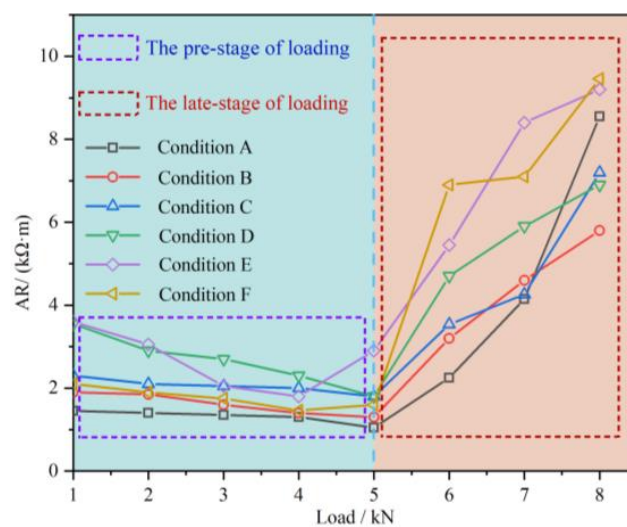


Figure 9. Relationship between load and AR of sample M-3.

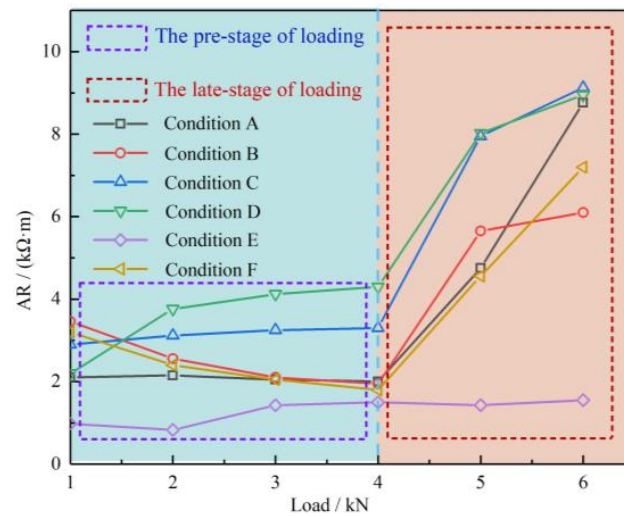


Figure 10. Relationship between load and AR of sample M-11.

As can be seen from Figures 8 and 10, although there are differences in the temporal evolution patterns of the AR high-resistance points of different coal samples, the overall change trends have reasonable similarity. On the whole, there are three main forms of high-resistivity point evolution:

(1) It develops from the low-resistivity point. In the initial loading stage, the change of AR resistance at the corresponding position is relatively stable and maintained at a low level. When loaded to a certain moment, its resistance value increases, indicating that the externally applied elastic strain energy accumulates in the weak unit surface inside the coal mass with increased load, forming a local stress concentration area. When the load exceeds its strength, the strain energy will be released outward, producing local rupture and gradually spreading with the increased stress.

(2) It evolves from the original high-resistance point. In the initial stage, the random distribution of the primary fractures inside the coal sample gradually closes with increased load, resulting in a slowly decreasing trend of AR at the corresponding location. However, when the load reaches a certain level, the resistance value of this part suddenly increases, producing a magnitude change, indicating that the primary fissures or defects that were closed start to redevelop under the influence of high stress, or new fissures are produced.

(3) Part of the original high-resistance point decreases to a lower level and no longer changes. This is caused by the non-homogeneity of the coal mass, in turn causing the bearing capacity of different parts of the coal sample to be strong or weak with the same load, which may lead to no further development of internal primary fissures or defects after closure.

From the AR tomography image and load curve, it can be seen that changes in the high-resistance points constitute the main controlling factor in the change in overall AR value. Furthermore, most of the high-resistance points show a changing trend of slowly decreasing, then sharply increasing with increased stress. The overall AR value should show the same rule, which indicates that the evolution of high-resistance points is mainly controlled by fracture propagation in the coal mass. In addition, it can be seen in the AR tomography image that the location of the final penetration damage of the coal sample coincides with the high-resistance area by comparing the physical maps of M-3 and M-11 after destruction (Figures 11 and 12). Therefore, the time and degree of fracture development at the corresponding location within the coal mass can be inferred from the variation pattern of AR at each point.



Figure 11. Photograph of sample M-3 after damage.



Figure 12. Photograph of sample M-11 after damage.

4. Discussion

4.1. Macro–Microscopic Mechanism Analysis of Resistivity Change of Loaded Coal Mass

A coal mass is an anisotropic non-homogeneous crystalline formation that develops under long-term complex conditions. The natural biochemical structure and composition and degree of water saturation have a significant influence on the original conductivity of coal mass and the type of conductivity (Figure 13) [22,23]. According to solid–dielectric theory, the electrical types of solid medium can be divided into two categories by the type of conductive carriers and the migration mode. One type is electron conductivity, generated by the directional movement of intermolecular electron clouds, and the other type is ion conductivity, caused by the migration of positive and negative ions in the filter-diffusion electric field in minerals and solutions [24]. The conductive properties of coal mass consist of both, but the electrical response of different aspects of coal differ in their sensitivity to the two conductivities in different incubation environments.

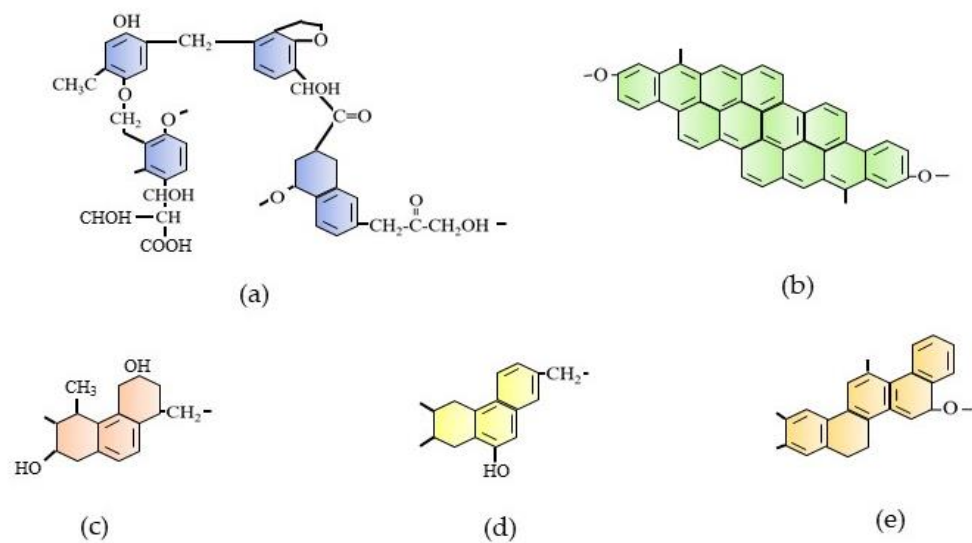


Figure 13. Structure model unit model of coal in different metamorphic grade: (a) lignite; (b) anthracite; (c) sub-bituminous coal; (d) high-volatility bituminous coal; (e) low-volatility bituminous coal.

For example, in the case of coal with low coalification, the internal aromatic nuclei of its molecules are filled with more interspersed polar oxygen-containing functional groups, which are arranged in a random and disordered cross-linked pattern through side chains and bridge bonds under the influence of van der Waals forces, resulting in weak electrical conductivity, dominated by the ionic conductivity type. For coal with high coalification, the internal functional groups account for a lower percentage. Due to the reduced cross-linking density, the polymerization capacity of the aromatic layer is improved and the internal molecular structure is more regular [25]. This arrangement also enhances the electron transport path and activity range, resulting in stronger electron conductivity than coal mass with low coalification. Therefore, the coal mass, a kind of solid dielectric, will interfere with the directional migration of internal carriers, thus generating current and breaking the equilibrium of the initial electric field in the native medium when carrying a certain load.

Take the ion-conducting coal mass shown in Figure 14, and assume that certain ions in the gap at the lowest potential energy level in the absence of external interference for thermal vibration will be in a semi-stable state, since the surrounding ions have a binding effect on them. If the ion wants to participate in the conductivity, it must break this binding effect. When the energy obtained by the external disturbance is greater than the binding energy, the ions will overcome the barrier and jump to another gap, and the diffusion process is accompanied by the generation of ion current. Here, it is assumed that ions with a vibrational frequency of ν at the lowest potential energy in semi-stable position A and B undergo thermal vibration (between the two points can be regarded as equipotential distribution), and the energy generated by the vibration obeys Boltzmann's distribution law. The ion is defined as n_0 . The binding potential barrier of adjacent ions is μ_0 [26]. Based on the above conditions, the number of ions that comfortably leap to the semi-stable position of another gap along a certain direction, overcoming the potential barrier per unit time, can be derived as:

$$n = \frac{n_0}{6} \quad (1)$$

The ion potential barrier in the gap does not remain in equilibrium under the action of electric field E . Ions migrate more easily if they conform to the direction of the electric field, and less easily if they don't conform to the direction of the electric field. Therefore,

the remaining number during the directional migration of ions along the direction of the electric field in unit time is:

$$\Delta n = n_{A \rightarrow B} - n_{B \rightarrow A} = \frac{n_0}{6} v e^{-\frac{u_0}{kT}} \left(e^{\frac{\Delta u}{kT}} - e^{-\frac{\Delta u}{kT}} \right) \quad (2)$$

In the presence of a weak electric field, it is:

$$\Delta u = \frac{1}{2} \delta q E \ll kT \quad (3)$$

$$e^{\pm \frac{\Delta u}{kT}} \approx 1 \pm \frac{\delta q E}{2kT} \quad (4)$$

This leads to the following formula:

$$\Delta n = \frac{n_0 q \delta v}{6kT} e^{-\frac{u_0}{kT}} \quad (5)$$

where q is the ionic charge and δ is the average leap distance.

The macroscopic average drift rate v of the ions along the electric field direction is:

$$v = \frac{q \delta^2 v}{6kT} e^{-\frac{u_0}{kT}} E \quad (6)$$

Combining the above equations yields ion mobility μ as:

$$\mu = \frac{q \delta^2 v}{6kT} e^{-\frac{u_0}{kT}} \quad (7)$$

The electrical conductivity γ of the dielectric is:

$$\gamma = \frac{n_0 q^2 \delta^2 v}{6kT} e^{-\frac{u_0}{kT}} \quad (8)$$

For electron conductivity, the expressions for mobility and conductivity were still derived through the ion conductivity expressions. The difference is that δ and n_0 in the electron conductivity expressions represent electron charge and average electronic transition distance, respectively. According to the analysis of the above equation, it can be seen that if the coal mass has not been damaged, the increased stress will cause compression of the space, restricting the free movement of ions between coal molecules, leading to decreased mobility and conductivity of ions, thus hindering the ion leap activity and resulting in increased resistivity. The performance of electrons is the opposite: the electron cloud links more closely before the coal molecules are disturbed by stress, which expands the range of electron transport. This makes the electron leap in the gap easier, so the mobility and conductivity of electrons increases, resulting in a decreasing trend of resistivity with increasing stress. In summary, the two conductivity mechanisms that contribute to the conductivity and resistivity changes of the coal mass under load are opposed. Therefore, to investigate the resistivity changes of coal mass under load, it is necessary to consider the weights of electron and ion conductivity in the conductivity of the coal mass, and to perform individual analyses for different coal qualities. In addition, based on the characteristics of the basic parameters of the tested coal samples and the variation law of AR with increasing stress, it can be noted that the conductivity of the coal mass with the sampling location is mainly dominated by electronic conductivity.

On the other hand, many studies have found that coal resistivity dominated by both electronic and ionic conductivity showed a significant increase after a certain time point when the coal mass was loaded at a high level [17–21]. This is because the high stress level intensifies the instability of the coal mass structure, the strain energy accumulated in the internal weak unit face in the early stage starts to release, and internal fissures develop

continuously and form a two-dimensional connection trend in the three-dimensional space. Due to the change in the conductive structure, the conductive medium in the space conducts current both in series and parallel with the fissure development direction. At this time, several conductive mechanisms play a role in the time series successively or simultaneously, and produce different behaviors near the fracture plane. Under the coupling effect, the electrical effect will evolve into mutual promotion and exclusion. The AR evolution tomography image and local AR variation of the samples show that the AR exhibits obvious anisotropic characteristics at the high-stress stage, and the high-resistance region produces a magnitude change relative to the background value. Comparing the morphology of the samples after peak damage reveals that the high-resistance region of all samples is generally consistent with the crack orientation after destabilization.

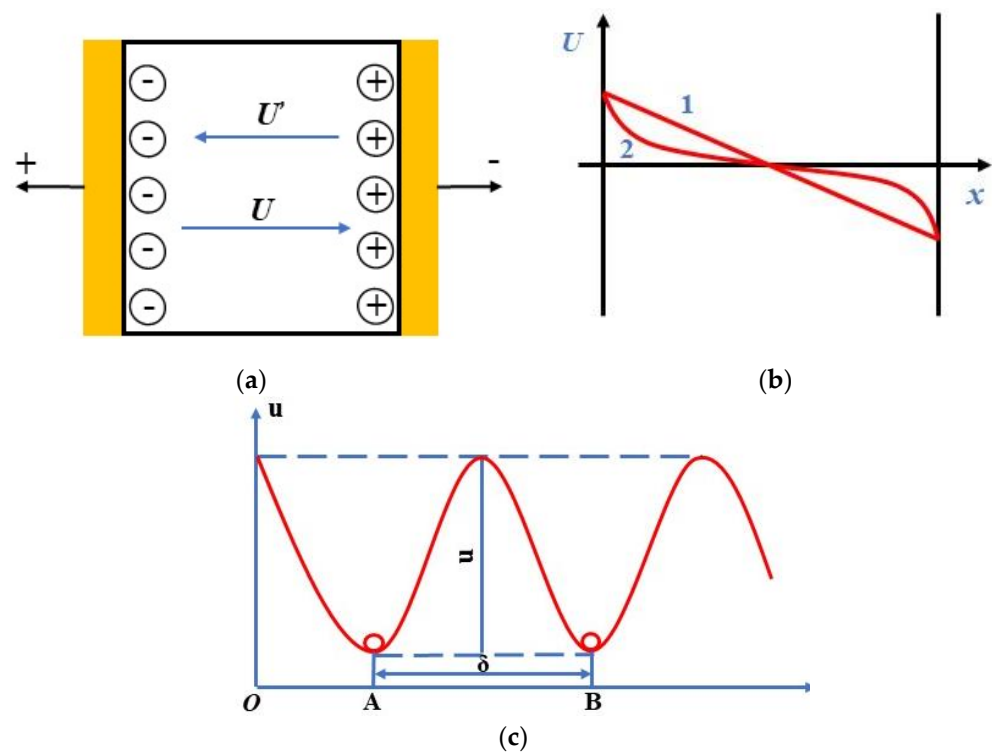


Figure 14. Electric field distribution caused by space charge of medium: (a) original potential distribution; (b) potential distribution after distortion; (c) ionic potential energy in solid medium.

The resistivity response of the coal mass during loading results from the interaction of multiple conductive mechanisms and is influenced by external factors such as electric field strength and test direction. In addition to its properties, the resistivity change of the coal mass during loading is still mainly contributed by the development of macroscopic fracture-conductive surfaces, which cannot hinder the overall resistivity trend even under the disturbance of the applied electric field.

4.2. Exploration of Joint AR-AE Response Method for Coal Rock Fracture Warning

Many scholars have studied the AE technique, and some of their results have been applied to the field of monitoring and forecasting coal dynamic disasters [27–32]. However, based on the feedback from experiments and engineering sites, there are still many bottlenecks hindering early warning by the AE technique. On the one hand, due to the complex geological conditions of an underground coal mine, the elastic stress wave generated by a coal mass during rupture will be irregularly attenuated by its anisotropy and non-homogeneity in the coal seam, which leads to a less strong final signal received by the AE instrument compared with the active source signal noise suppression. In addition, the AE signal is not received far enough ahead of time, i.e., the damage has already occurred

when the signal is received. On the other hand, although the resistivity method has a strong ability to distinguish the geological information of the detection area, it is limited by the construction conditions and sampling frequency, and cannot monitor the target area in real time as the AE technique does. Based on the abovementioned factors and the measured experimental results, the characteristics of AE and AR tomography during the process of loading the coal sample were further studied qualitatively. Additionally, passive monitoring–active detection, i.e., the integrated AR–AE technique, for early warning of coal or rock failure disaster was proposed.

The high AE counts and fluctuation degree were used to determine the loaded stage of the coal mass. From the previous experimental results, it can be seen that AE has the characteristics of low amplitude, small amplitude, and continuous fluctuation in the low load-bearing stage. In the middle load stage, the AE signal is relatively active, presenting irregular discrete signal characteristics and a pulse peak higher than 5000. In the high-stress stage, the AE counts show high amplitude, burst-type behavior, and more intensity. In addition, the characteristics of AE counts in the constant load stage are apparent, and all of them have a certain window. It is known from the previous study that sample M–3 still had a small number of AE signals even in the steady pressure stage when it was finally close to destruction, which indicates that coal mass can be subjected to a high degree of load, and the maintenance of stress still causes coal mass fracture expansion and nucleation. The AE signals of sample M-11 had a short calm period before the stress reached the peak. All of the above characteristics can be captured as precursor signals of coal mass destabilization.

The spatiotemporal evolution characteristics of AR tomography were used to identify the internal fracture sources of coal mass. Due to the heterogeneity of coal mass, the load-bearing capacity of different internal parts varies even under the same loaded conditions, so the fracture evolution characteristics also differ, as well as the internal conductive structure evolution. However, it can be seen from the AR tomography images and temporal variation characteristics that the temporal variation characteristics of the loaded coal mass can reflect the local variation and loading state to a certain extent. Combined with the resistivity variation mechanism of the loaded coal mass, the conductive type of coal mass can be obtained, while the spatial variation characteristics can invert the internal stress concentration area, fracture location, and development state. A comprehensive analysis of both can invert the location of the rupture source, which can provide a basis for determining early warning and prevention areas at engineering sites.

The above results show that both acoustic and electrical signals during the loading of the coal mass are controlled by the mechanical behavior. Meanwhile, the strength of the AE signal not only reflects the internal rupture level of the coal mass, but also has a highly positive correlation with the degree of AR change. Through comparative analysis, it can be found that after the AE signal becomes active and appears with high-value pulses greater than 5000 and less than 8000, the overall resistance value of the AR tomography image will show an order of magnitude change, indicating that the coal mass may have entered the destabilization state, which is defined as a secondary warning response. The AE signal appears to be a calm or small dense signal after exhibiting pulse values greater than 8000. At the same time, the high-resistance area of the AR develops to fill the interior of the tomography image, which indicates that damage is coming, and this is defined as the first-level warning response.

In view of the above factors, AE signal amplitude and variation characteristics can be used to monitor the loading state of coal during the whole process of engineering field application, and phased detection apparent resistance tomography images can be used to locate the source of rupture and make a secondary judgment of the loading state.

5. Conclusions

(1) In the process of multi-step loading, the AR and AE signals of coal samples have good correspondence with the load changes. At the early stage of loading, the primary fracture gradually closes under pressure, the original high-resistivity area and overall

resistance value of the sample gradually decrease, and AE is maintained at a low level. The maximum value is reached near the stress peak.

(2) The AR changes in each region during the loading process of coal samples are anisotropic, and the spatial and temporal evolution characteristics of the internal high-resistance region can indirectly reflect the degree and location of fracture development in coal samples. In addition, areas with small AR in the early loading period are more likely to form stress concentration areas and produce deformation and rupture when the loading degree is higher. Therefore, field applications should be focused on areas with these two kinds of AR variation characteristics.

(3) From the microscopic point of view, the coal mass can be regarded as a solid dielectric with both ionic and electronic conductivity, and its natural biochemical structure and composition determine which conductive property is dominant. If ionic conductivity is dominant, the resistivity of the loaded coal mass will increase with stress before damage occurs, while the opposite is true if electronic conductivity is dominant. From the macroscopic point of view, the resistivity change of the loaded coal mass is influenced by the evolution of its internal structure, and the development of its fissure-conductive surface represents the main contribution to the electrical property change.

(4) Before coal mass rupture, AE and AR signals exist with different precursor characteristics. For application at engineering sites, the AE method as a means of passive monitoring can continuously monitor the test area and obtain the degree of coal mass loading through temporal signal changes. With the resistivity method, as an active means of detection, the temporal and spatial changes of AR characteristics can invert and locate the stress concentration area and rupture source, and the two parts of precursor information can verify and complement each other.

Author Contributions: Conceptualization, X.W. and F.C.; methodology, X.W.; software, H.T.; formal analysis, X.W.; investigation, B.M. and H.T.; data curation, B.M.; writing—original draft preparation, X.W.; writing—review and editing, G.Z., D.C. and B.M.; supervision, F.C. All authors have read and agreed to the published version of the manuscript.

Funding: This research received no external funding.

Institutional Review Board Statement: Not applicable.

Informed Consent Statement: Not applicable.

Data Availability Statement: Data is available on request from the authors.

Conflicts of Interest: The authors declare no conflict of interest.

References

1. Kai, W.; Feng, D. Coal-gas compound dynamic disasters in china: A review. *Process Saf. Environ.* **2020**, *133*, 1–17.
2. Wang, E.; Zhang, G.; Zhang, C.; Li, Z. Research progress and prospect on theory and technology for coal and gas outburst control and protection in china. *J. China Coal Soc.* **2022**, *47*, 297–322.
3. Li, X.; Chen, S.; Wang, S.; Zhao, M.; Liu, H. Study on in situ stress distribution law of the deep mine: Taking linyi mining area as an example. *Adv. Mater. Sci. Eng.* **2021**, *2021*, 5594181. [[CrossRef](#)]
4. Li, Z.; Zhang, X.; Wei, Y.; Ali, M. Experimental study of electric potential response characteristics of different lithological samples subject to uniaxial loading. *Rock Mech. Rock Eng.* **2021**, *54*, 397–408. [[CrossRef](#)]
5. Yuan, L. Research progress of mining response and disaster prevention and control in deep coal mines. *J. China Coal Soc.* **2021**, *46*, 716–725.
6. Qiu, L.; Liu, Z.; Wang, E.; He, X.; Feng, J.; Li, B. Early-warning of rock burst in coal mine by low-frequency electromagnetic radiation. *Eng. Geol.* **2020**, *279*, 105755. [[CrossRef](#)]
7. Niu, Y.; Wang, E.; Li, Z.; Gao, F.; Zhang, Z.; Li, B.; Zhang, X. Identification of coal and gas outburst-hazardous zones by electric potential inversion during mining process in deep coal seam. *Rock Mech. Rock Eng.* **2022**, *55*, 3439–3450. [[CrossRef](#)]
8. He, M.C.; Miao, J.L.; Feng, J.L. Rock burst process of limestone and its acoustic emission characteristics under true-triaxial unloading conditions. *Int. J. Rock Mech. Min.* **2010**, *47*, 286–298. [[CrossRef](#)]
9. Jia, Z.; Xie, H.; Zhang, R.; Li, C.; Zhang, Z. Acoustic emission characteristics and damage evolution of coal at different depths under triaxial compression. *Rock Mech. Rock Eng.* **2020**, *53*, 2063–2076. [[CrossRef](#)]

10. Li, X.; Chen, S.; Liu, S.; Li, Z. Ae waveform characteristics of rock mass under uniaxial loading based on hilbert-huang transform. *J. Cent. South Univ.* **2021**, *28*, 1843–1856. [[CrossRef](#)]
11. Dou, L.; Yang, K.; Chi, X. Fracture behavior and acoustic emission characteristics of sandstone samples with inclined precracks. *Int. J. Coal Sci. Technol.* **2020**, *28*, 1843–1856. [[CrossRef](#)]
12. Zhang, R.; Liu, J.; Sa, Z.; Wang, Z.; Wang, C. Experimental investigation on multi-fractal characteristics of acoustic emission of coal samples subjected to true triaxial loading-unloading. *Fractals* **2020**, *28*, 2050092. [[CrossRef](#)]
13. Feng, X.; Ding, Z.; Ju, Y.; Zhang, Q.; Ali, M. “double peak” of dynamic strengths and acoustic emission responses of coal masses under dynamic loading. *Nat. Resour. Res.* **2022**, *31*, 1705–1720. [[CrossRef](#)]
14. Kong, X.; Wang, E.; Hu, S.; Shen, R.; Zhan, T. Fractal characteristics and acoustic emission of coal containing methane in triaxial compression failure. *J. Appl. Geophys.* **2016**, *124*, 139–147. [[CrossRef](#)]
15. Li, H.; Qiao, Y.; Shen, R.; He, M.; Cheng, T.; Xiao, Y.; Tang, J. Effect of water on mechanical behavior and acoustic emission response of sandstone during loading process: Phenomenon and mechanism. *Eng. Geol.* **2021**, *294*, 106386. [[CrossRef](#)]
16. Wang, X.; Asem, P.; Hu, C.; Labuz, J.F. Microcracking in tensile fracture of a brittle rock. *Eng. Fract. Mech.* **2021**, *251*, 107789. [[CrossRef](#)]
17. Jiang, W.; Liu, Y. Study on variation of electrical resistivity under uniaxial pressure environment for rocks. *J. Geol.* **2009**, *33*, 299–302.
18. Li, S.; Xu, X.; Liu, Z.; Yang, W.; Xu, L. Electrical resistivity and acoustic emission response characteristics and damage evolution of sandstone during whole process of uniaxial compression. *Chin. J. Rock Mech. Eng.* **2014**, *33*, 14–23. [[CrossRef](#)]
19. Jia, P.; Lei, L.L.; Liu, D.Q.; Wang, X.S.; Wang, D.C. Insight into rock crack propagation from resistivity and ultrasonic wave variation. *Theor. Appl. Fract. Mec.* **2020**, *109*, 102758. [[CrossRef](#)]
20. Liu, Q.; Qiu, L.; Zu, Z.; Wei, S.; Cheng, X.; Yin, S. Variation characteristics of apparent resistivity of fractured coal sample in loading process. *J. Xi'an Univ. Sci. Technol.* **2021**, *41*, 731–738.
21. Xu, X.; Liu, B.; Li, S.; Song, J.; Li, M.; Mei, J. The electrical resistivity and acoustic emission response law and damage evolution of limestone in brazilian split test. *Adv. Mater. Sci. Eng.* **2016**, *2016*, 8052972. [[CrossRef](#)]
22. Shi, Q.; Qin, Y.; Chen, Y. Relationship between thermal conductivity and chemical structures of chinese coals. *ACS Omega* **2020**, *5*, 18424–18431. [[CrossRef](#)] [[PubMed](#)]
23. Liu, X.; Wang, L.; Kong, X.; Ma, Z.; Nie, B.; Song, D.; Yang, T. Role of pore irregularity in methane desorption capacity of coking coal. *Fuel* **2022**, *314*, 123037. [[CrossRef](#)]
24. Liu, Z.; Wang, W.; Yang, J.; Shi, M.; Ma, T.; Wang, D.; Yang, H. Review and prospect of study on conductive properties of coal and cbm reservoirs. *Prog. Geophys.* **2020**, *35*, 1415–1423.
25. Lin, B.; Zha, W.; Liu, T. Experimental study on molecular structure differences between the tectonic coal and primary coal in pingdingshan coalfield. *Vib. Spectrosc.* **2019**, *103*, 102930. [[CrossRef](#)]
26. Chen, P. Direct Current Electric Method Response of Regional Coal and Gas Outburst Danger and Its Application. Doctor Thesis, China University of Mining and Technology, Xuzhou, China, 2013.
27. Wang, X.; Wang, E.; Liu, X.; Zhou, X. Failure mechanism of fractured rock and associated acoustic behaviors under different loading rates. *Eng. Fract. Mech.* **2021**, *247*, 107674. [[CrossRef](#)]
28. Qiu, P.; Ning, J.; Wang, J.; Hu, S.; Li, Z. Mitigating rock burst hazard in deep coal mines insight from dredging concentrated stress: A case study. *Tunn. Undergr. Sp. Technol.* **2021**, *115*, 104060. [[CrossRef](#)]
29. Chen, X.; Li, W.; Yan, X. Analysis on rock burst danger when fully-mechanized caving coal face passed fault with deep mining. *Saf. Sci.* **2012**, *50*, 645–648. [[CrossRef](#)]
30. Lu, C.; Dou, L.; Zhang, N.; Xue, J.; Wang, X.; Liu, H.; Zhang, J. Microseismic frequency-spectrum evolutionary rule of rockburst triggered by roof fall. *Int. J. Rock Mech. Min.* **2013**, *64*, 6–16. [[CrossRef](#)]
31. Li, D.; Wang, E.; Kong, X.; Ali, M.; Wang, D. Mechanical behaviors and acoustic emission fractal characteristics of coal specimens with a pre-existing flaw of various inclinations under uniaxial compression. *Int. J. Rock Mech. Min.* **2019**, *116*, 38–51. [[CrossRef](#)]
32. Qiu, L.; Zhu, Y.; Song, D.; He, X.; Wang, W.; Liu, Y.; Xiao, Y.; Wei, M.; Yin, S.; Liu, Q. Study on the nonlinear characteristics of emr and ae during coal splitting tests. *Minerals* **2022**, *12*, 108. [[CrossRef](#)]